Energy Storage Materials 15 (2018) 415–421

Contents lists available at ScienceDirect

Energy Storage Materials

journal homepage: www.elsevier.com/locate/ensm

Dendrite-free and minimum volume change Li metal anode achieved by three-dimensional artificial interlayers

Yang Zhao[a], Xiaofei Yang[a], Qian Sun[a], Xuejie Gao[a], Xiaoting Lin[a], Changhong Wang[a], Feipeng Zhao[a], Yipeng Sun[a], Keegan R. Adair[a], Ruying Li[a], Mei Cai[b], Xueliang Sun[a,*]

[a] Department of Mechanical and Materials Engineering, University of Western Ontario, London, Ontario, Canada N6A 5B9
[b] General Motors R & D Center, Warren 48090-9055, MI, USA

ARTICLE INFO

Keywords:
Li metal anode
3D interlayer
Dendrite-free
Minimum-volume-change

ABSTRACT

Li metal anodes are considered as the "Holy Grail" for the next-generation Li metal batteries due to their unique properties such as high specific capacity, low potential, and light weight. However, Li metal anodes have serious challenges to be overcome, including Li dendrite growth, "dead Li" layer formation, and infinite volume change during the repeated plating and stripping. Herein, we extend the "interlayer" concept to the application of Li metal anodes and rationally design a bi-functional interlayer. The vertical nitrogen-doped carbon nanotubes (NCNTs) are grown on the carbon fibre of carbon papers (CP) to obtain a 3D interlayer for Li metal. Firstly, we demonstrate the relationship between surface area and electrochemical performances on the 3D structure by controlling the growth time of NCNTs. Remarkably, the Li-CP-NCNTs composite electrode can deliver very stable performances over 600 h (~ 900 cycles) and 250 h (~ 750 cycles) at the ultrahigh current densities of 5 mA cm^{-2} and 10 mA cm^{-2}, respectively, which is two times higher than that of the cell using pristine CP interlayers. Meanwhile, with a high capacity of 3 mAh cm^{-2}, the Li metal anode with CP-NCNTs interlayer delivers a long life time of over 350 h at a current density of 3 mA cm^{-2}. The morphologies of both Li foil and CP-NCNTs interlayers display dendrite-free deposition and minimum volume change. We believe that these new findings could open a new avenue for achieving long life time, dendrite-free and minimal volume change Li metal anodes.

1. Introduction

In the past years, Li-ion batteries (LIBs) have been considered as one of the most successfully developed energy storage devices for portable electronics, electric cars, and large scale energy storage stations. LIBs possess many outstanding features, including high energy density, no memory effect, low maintenance, and minimal self-discharge [1]. However, the growing requirements for better LIBs require constant progress in terms of improved safety, longer lifetime, smaller size, lighter weight, and lower cost. The next generation Li metal batteries (LMBs) such as Li-S, Li-air, and all-solid-state batteries, have recently received more attention due to their higher energy densities [2,3]. As an ideal anode material candidate, Li metal has unique properties such as high theoretical capacity (3860 mAh g^{-1}), low electrochemical potential (−3.04 V vs. the standard hydrogen electrode), and light weight (0.53 g cm^{-3}) [4,5]. Although Li metal is considered to be the "Holy Grail" of anode materials, it still has several challenges to be addressed before Commercialization. During the repeated electrochemical plating/stripping process, mossy and dendritic structures are formed on the surface of the Li electrode [6–8]. Furthermore, the Li dendrites may penetrate the separator and cause internal short circuits, leading to serious safety concerns. In addition, "dead Li" is formed from the mossy and dendritic Li, which is electrochemical inactive due to the loss of electrical contact and blocking of the Li^+/electron transportation between the electrolyte and bulk Li [9,10]. During the electrochemical cycling process, side reactions between the electrolyte and metallic Li lead to the formation of solid electrolyte interphase (SEI) layers on the surface of Li metal. The unstable "SEI" will lead to a non-uniform Li ionic flux, resulting in Li dendrite growth [11,12]. Meanwhile, the repeated breaking and repair of the SEI during cycling will cause the depletion of the electrolyte and Li, which will lower the coulombic efficiency (CE) and shorten the life time of the Li metal anode [13]. Another serious issue of Li metal is the infinite volume change due to its "hostless" nature, which will also significantly affect the performances of the Li metal anode and LMBs [14,15].

* Corresponding author.
E-mail address: xsun@eng.uwo.ca (X. Sun).

https://doi.org/10.1016/j.ensm.2018.07.015
Received 5 June 2018; Received in revised form 16 July 2018; Accepted 20 July 2018
Available online 21 July 2018

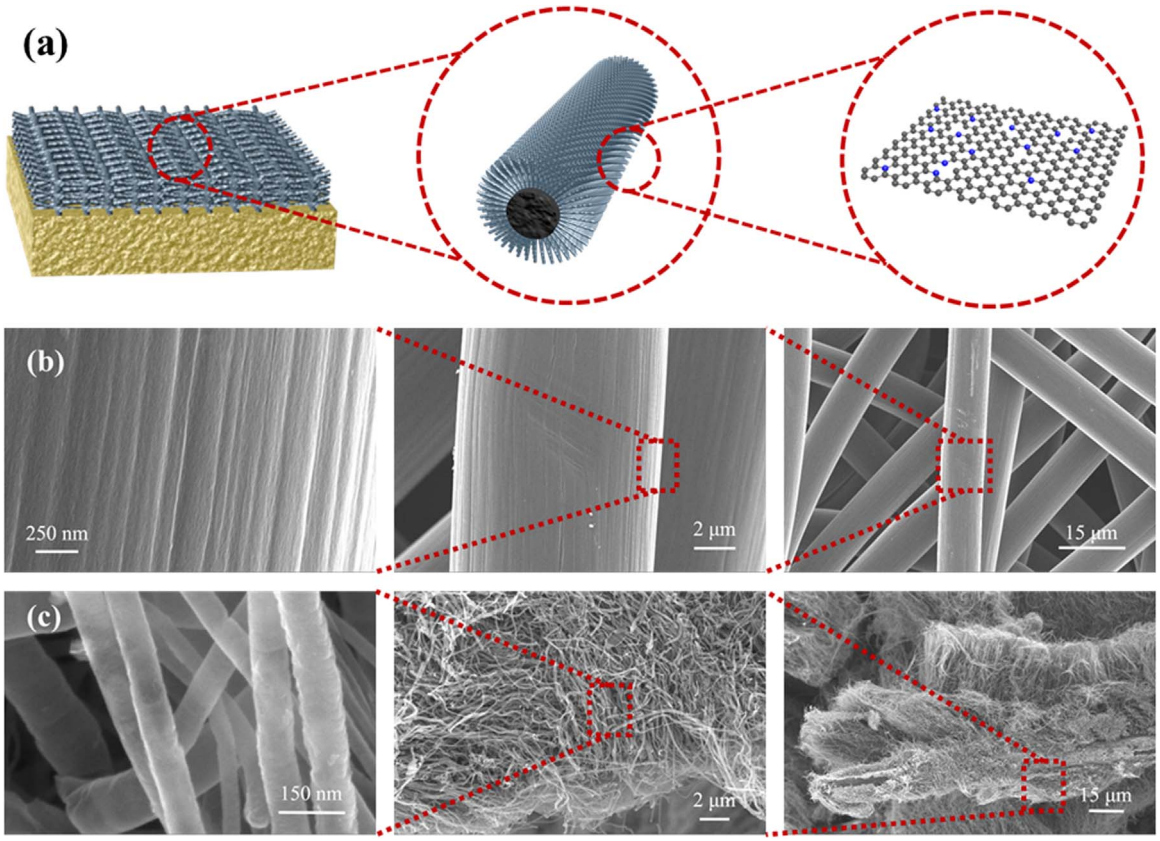

Fig. 1. (a) Schematic diagram of the configuration using CP-NCNTs as interlayer for Li metal anode; (b) SEM images of pristine carbon paper; (c) SEM images of CP-NCNTs interlayers.

In recent years there have been many approaches proposed to stabilize the Li anode. The stable formation of SEI is one of the key factors to suppressing Li dendrite growth and improving life time, in which both in-situ and ex-situ procedures have been reported [16]. The modification of electrolyte components, including Li salts, organic solvents, and additives, is an effective strategy to obtain a stable SEI during the electrochemical plating/stripping process [3]. Alternatively, surface coating/modification on the Li metal has been explored as another approach to stabilize the SEI layer as an ex-situ process [17]. Various materials and thin films have been synthesized or deposited on the Li metal anode as protective layers, such as Al_2O_3, alucone, Li_3PO_4, Li_3PS_4, and $Li_{13}In_{13}$ alloy [18–24]. The robust protective layers can prevent side reactions between liquid electrolyte and Li metal, generate homogeneous Li^+ flux, and reduce the Li dendrite growth. Furthermore, a thermal infusion method of melting Li into 3D hosts was developed by Cui's group as a prominent approach to address the “infinite volume change” of the Li metal anode [25–28]. Different materials have been used as 3D hosts for Li metal, including metal foams, Li-ion conductive matrix, carbon-based matrices, and enabling minimum volume change and longer life times [29–32]. Especially, the carbon fiber based materials received increasing attention. Fox example, Lu et al. demonstrates the carbon paper (CP) with sponge carbon layer (SCCP) as the skeletons for Li metal anode [33]. The additional sponge carbon layer with low electronic conductivity and compact structure enables the uniform Li deposition in the 3D matrix and suppresses the dendrite growth. Furthermore, different modifications on CP, such as sliver layer and graphene nanosheets, have been reported to improve the electrochemical performances of the CP [34,35]. However, there are still some limitations for the thermal infusion method, in which one concern is the high temperature (generally higher than the melting point of Li (180 °C)) process that requires specialized fabrication and is uneconomical. Another shortage is the stringent requirements of the Li wettability on the surface of hosts. Therefore, there are still many remaining challenges for 3D Li composites prepared via thermal infusion method for practical applications in future battery systems.

Recently, we proposed the idea of conductive interlayers (CP) for Li metal anodes with a facile fabrication process [36]. The concept of the “interlayer” was firstly demonstrated by Manthiram's group where they placed an interlayer between the cathode and separator for Li-S batteries to trap soluble polysulfide intermediates, providing space to store electrolyte and reaction production [37]. Here we extend the interlayer concept to Li metal anode protection, which can significantly enhance the electrochemical plating/stripping performances and suppress the dendrite growth. It is believed that the bi-functional interlayer can not only enable a uniform Li^+ flux on the surface of Li metal, but also serve as the host for Li deposition and restrict the volume change of the Li metal anode spontaneously. However, the reported conductive interlayer is still not good enough under high current density with high capacities for practical applications [36,38,39]. Meanwhile, the factors affecting the electrochemical performance of the conductive interlayers are unclear. It is also worth to mention that the introduction of an interlayer may decrease both the gravimetric and volumetric energy density of batteries. In this case, the density and thickness of interlayer design is an important factor affecting the gravimetric and volumetric energy density of the cells.

Herein, we demonstrate a bi-functional interlayer using CP as a base material for Li metal anode. The vertically aligned N-doped carbon nanotubes (NCNTs) are grown on the CP to achieve a 3D interlayer structure, named CP-NCNTs. By controlling the time for NCNTs growth, the surface areas of the CP-NCNTs are adjusted, and is related to the electrochemical performances. Promisingly, the design of the CP-NCNTs interlayer can enhance the electrochemical performances and achieve over 600 h cycling time at a high current density of 5 mA cm^{-2}. Meanwhile, with a high capacity of 3 mAh cm^{-2}, the Li metal electrode with CP-NCNTs interlayer delivers a long life time of

over 350 h at a current density of 3 mA cm^{-2}. Benefitting from the bi-functional interlayer, both the Li dendrite growth and the volume change have been effectively relieved simultaneously. These new findings could open a new window for the fabrication of safe, long life time, dendrite-free and minimum volume change Li metal anodes.

2. Results and discussion

The configuration of the Li metal electrode using CP-NCNTs as an interlayer is shown in Fig. 1 **(a)**. The CP-NCNTs was put directly on the surface of Li foil (between Li and separators) with the same diameter, and the composite electrodes were used together as the anode. Fig. 1**(b)** displays the SEM images of pristine carbon papers. It can be seen that the pristine CP consists of carbon fibres with diameters of ~ 8 μm. The surfaces of the carbon fibres in CP are relatively smooth with some wrinkles. To fabricate the CP-NCNT interlayers, NCNTs were grown on the CP through a one-step spray pyrolysis chemical vapor deposition (SPCVD) method, which was reported in our previous works [40]. Fig. 1 **(c)** and Fig. S1 present the SEM images of CP-NCNTs after SPCVP process. It can be observed that the carbon fibers in CP are totally covered with vertical and dense NCNTs. The lengths and diameters of the NCNTs are around 30 μm and 100 nm, respectively. From the cross-section images in Fig. S1, the NCNTs are not only distributed on the surface of CP, but also grown in the inner space of CP.

To understand the relationships between the surface area and electrochemical performances of CP-NCNTs interlayers, the growth times of NCNTs were controlled during the SPCVD process. Different SPCVD times of 10 min, 20 min, and 30 min were carried out for the samples named CP-NCNTs-1, CP-NCNTs-2, and CP-NCNTs-3, respectively. Fig. S2 **(a)** shows the N_2 adsorption/desorption isotherms for CP-NCNTs-1, CP-NCNTs-2 and CP-NCNTs-3. From the BET analysis, the surface areas of CP-NCNTs-1 to CP-NCNTs-3 increase with SPCVD reaction times, which are 19.8, 20.9, 25.3 $m^2 g^{-1}$, respectively. Fig. S2 **(b)** displays the pore size distributions of the three samples, indicating the similar pore distribution with the average pores widths of about 8 nm. Fig. S3 shows the Raman spectra of CP-NCNTs-1, CP-NCNTs-2, and CP-NCNTs-3. In the Raman spectra, the peak at about 1591 cm^{-1} (G band) is related to the vibration of sp2 bonded carbon atom in 2D hexagonal lattice and the 1329 cm^{-1} (D band) is related to the defects and disorder in the hexagonal graphitic layers. The I_D/I_G of CP-NCNTs-3 is about 0.73, which is lower than that of 0.90 for CP-NCNTs-1 and CP-NCNTs-2. Meanwhile, it has been proven in our previous studies that the N-content of the CP-NCNTs-3 is about 4% with the three types of N bonding structures, including pyridinic-N, pyrrolic-N, and graphitic-N[35].

To evaluate the influence of the interlayer on the electrochemical performances, symmetrical coin cells (2032-type) with two identical Li-interlayers were assembled using a $LiPF_6$ contained carbonate-based electrolyte (1 M $LiPF_6$ in EC/DEC/DMC in 1: 1: 1 vol%). Two types of interlayers have been investigated for comparison: single layer of CP and single layer of CP-NCNTs. From our previous work, the use of only single layer of CP as an interlayer can improve the electrochemical performances over the bare Li foil, however, the life time and cycling stability at high current density are still insufficient [33]. Fig. 2 shows the electrochemical plating/stripping performances of the Li foil with one layer of CP (named as *Li-CP*) and CP-NCNTs-3 (named as *Li-CP-NCNTs-3*) as interlayers under different current densities with different capacity limits. Fig. 2 **(a)** exhibits the cycling stability and detailed voltage profiles of Li-CP and Li-CP-NCNTs-3 at a current density of 5 mA cm^{-2} with a capacity limit of 1 mAh cm^{-2}. From the cycling stability tests, the over-potential of Li-CP starts to increase after 200 h (~ 330 cycles) and rises to over 2000 mV (versus Li^+/Li) after 350 h (~600 cycles) with large polarization in the voltage profiles. Meanwhile, from our previous study, the bare Li foil failed after only 50 h at such high current density [33]. In comparison, Li-CP-NCNTs-3 can maintain superior stability and lower over-potentials of 200 mV (versus Li^+/Li) after 350 h (~600 cycles). Even after 580 h (~900 cycles), the over-potential of Li-CP-NCNTs-3 is only about 250 mV (versus Li^+/Li), illustrating the enhanced electrochemical performance enabled by the CP-NCNTs interlayer. When increasing the current density to 10 mA cm^{-2}, the over-potential of Li-CP starts to increase after only 75 h (~200 cycles) and rises up to over 3000 mV (versus Li^+/Li) after 180 h (~500 cycles), as shown in Fig. 2 **(b)**. The fluctuating voltage profiles are related to the Li dendrite (mossy) growth, dead Li layer formation and inner short circuiting. Remarkably, the Li-CP-NCNTs-3 can be stable for over 250 h (~750 cycles) at a very high current density of 10 mA cm^{-2}. The results show that with the modification of NCNTs on CP, the stability of the Li-CP-NCNTs can be significantly improved even at ultrahigh current density.

Recently, researchers have come to a consensus that the regular testing parameter of 1 mAh cm^{-2} cannot meet the requirements for practical applications and does not highlight the potential of large capacity Li metal anodes [36]. To demonstrate the use of CP-NCNTs interlayers with a practical cycling capacity, the performance of symmetric cells with large capacities of 3 mAh cm^{-2} and 5 mAh cm^{-2} was explored. Fig. 2 **(c)** presents the cycling stability and voltage profiles of Li-CP and Li-CP-NCNTs-3 using a high current density of 3 mA cm^{-2} and high capacity limit of 3 mAh cm^{-2}. At this condition, the stability of bare Li foil is very poor and overpotential of Li starts to increase after only 35 h. It can be seen that the CP interlayer alone can only stabilize the performances for about 130 h with the over-potential increasing to 1000 mV (versus Li^+/Li) after 180 h. However, the Li-CP-NCNTs-3 maintains a stable cycling performance with an over-potential of only 450 mV after 350 h, which is almost double the life time of the pristine CP interlayer. After further increasing the current density to 5 mA cm^{-2} with a high capacity of 3 mAh cm^{-2}, the over-potential of the Li-CP begins to increase only after 100 h, however, the Li-CP-NCNTs-3 can be stabilized over 140 h, as shown in Fig. 2 **(d)**. Fig. S4 displays the cycling performance of Li-CP and Li-CP-NCNTs-3 at current densities of 3 mA cm^{-2} and 5 mA cm^{-2} with an ultrahigh capacity of 5 mAh cm^{-2}. The results indicate that even with a high capacity of 5 mAh cm^{-2}, the Li-CP-NCNTs-3 can still provide significantly improved stability and cycling performances compared to Li-CP. Furthermore, the electrochemical results show that the vertical NCNTs can make a significant influence on the performance of high capacity Li metal anodes even at high current densities.

To understand the influence of surface area on the electrochemical performances of the CP-NCNTs interlayers, different electrodes consisting of Li-CP-NCNTs-1, Li-CP-NCNTs-2, and Li-CP-NCNTs-3 were investigated in symmetrical coin cells. Fig. S5 shows the comparison of the cycling stability of Li-CP-NCNTs-1, Li-CP-NCNTs-2 and Li-CP-NCNTs-3 at the current density of 2 mA cm^{-2} with a capacity of 2 mAh cm^{-2}. It can be observed that all of the samples used as interlayers can effectively enhance the electrochemical performances of the Li metal anode. Furthermore, with an increase of surface area, better performances are achieved for the Li-CP-NCNTs-3. For example, the over-potentials of Li-CP-NCNTs-1, Li-CP-NCNTs-2 and Li-CP-NCNTs-3 are about 250 mV, 200 mV and 150 mV after 225 h, respectively. Fig. S6 displays the cycling performances of Li-CP-NCNTs-1 and Li-CP-NCNTs–2 at a higher current density of 3 mA cm^{-2} with a capacity of 3 mAh cm^{-2}. The results show a similar trend, in which the samples with higher surface area indicate better electrochemical stabilities. These results can be rationalized by the high surface area lowering the local current on the interlayer, leading to a more homogeneous electron/Li^+ distribution with reduced the Li dendrite growth. Meanwhile, the density of CP-NCNTs is around 0.66 g cm^{-3}, which can be considered as the light materials compared with various metal-based interlayer and host for Li metal anode, such Ni, Cu, et al. Thus, the gravimetric energy density using CP-NCNTs interlayer will be higher than the metal-based interlayer and host. Then, in our previous study [36], 5 layer of CP are required using as interlayer for Li metal

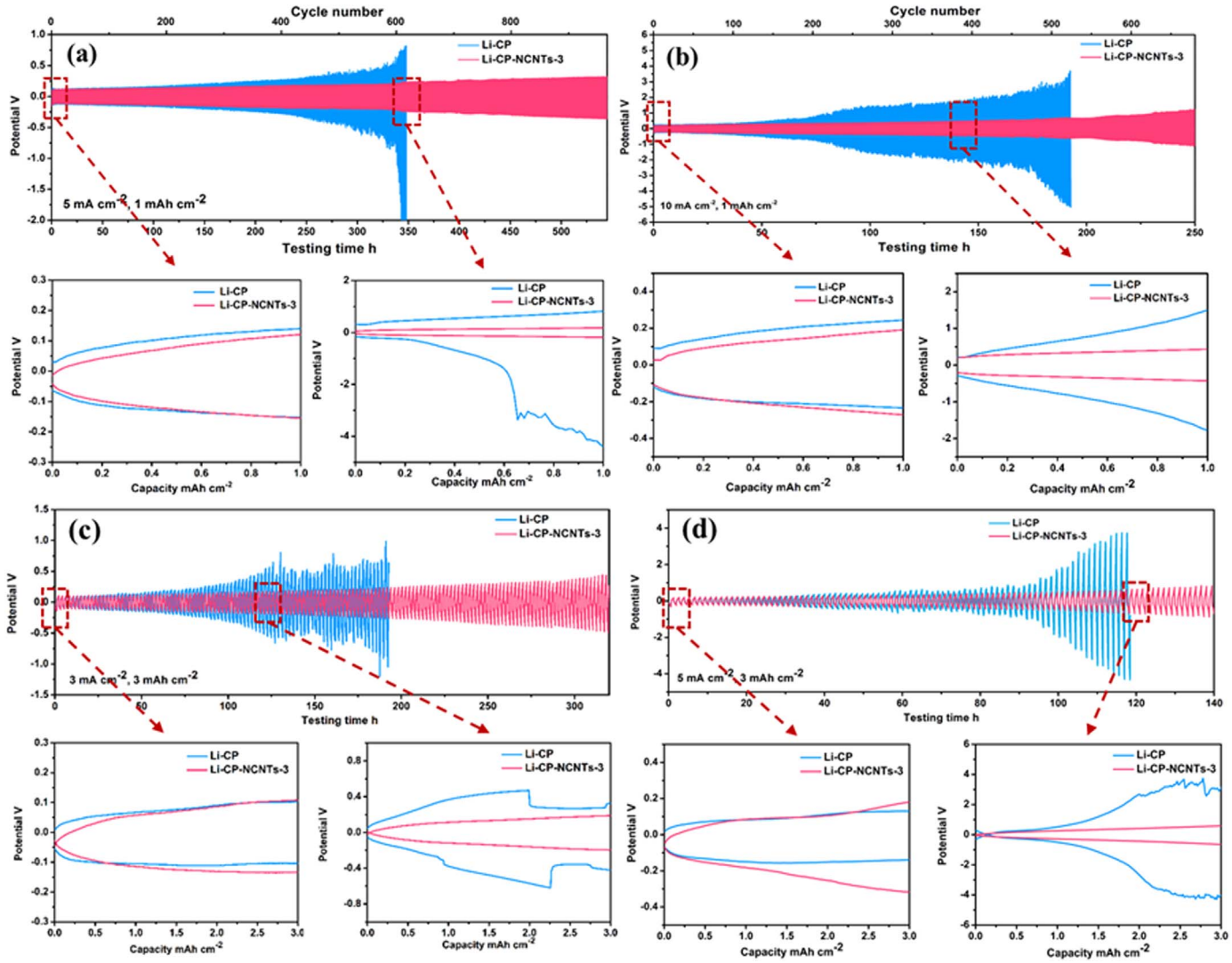

Fig. 2. Comparison of the cycling stability of the Li-CP and Li-CP-NCNTs-3 at a current density of 5 mA cm^{-2} (a), 10 mA cm^{-2} (b) with the capacity limit of 1 mAh cm^{-2}; and at the current density of 3 mA cm^{-2} (c), 5 mA cm^{-2} (d) with the capacity limit of 3 mAh cm^{-2}.

anode to maintain the stable electrochemical performances under high current density and high capacity. Typically, the weight and thickness of 5 layer of CP are 0.05 g and 1050 μm, respectively. After grown NCNTs, the weight and thickness of CP-NCNTs is only 0.019 g and 400–450 μm, respectively. Promisingly, the CP-NCNTs interlayer can maintain very stable performances under high current density and high capacity. In this case, with the design of CP-NCNTs, both volumetric and gravimetric energy density using CP-NCNTs are much higher than that of multi-layer of CP.

To demonstrate the bi-functional properties of the interlayer design, a second configuration of the use of CP-NCNTs for Li metal batteries has been also fabricated and examined. In this case, all the designed interlayers have also been investigated as substrates for Li deposition. The cycling Coulombic efficiencies (CE) of Cu foil, CP and CP-NCNTs were carried out under different cycling conditions, as shown in Fig. 3. All cells containing CP and CP-NCNTs have been activated and stabilized in the first 10 cycles in the voltage range of 0–2 V. From Fig. 3**(a)**, the Cu foil delivers a low initial CE of ~ 80% and decreases to only 40% after 100 cycles. Promisingly, both the CP and CP-NCNTs display better CE than the Cu foil, in which the CE of CP drops to 70% after 280 cycles, however, the CP-NCNTs can maintain a high CE of 99.5%. When increasing the current density to 3 mA cm^{-2} or capacity to 3 mAh cm^{-2} (as shown in Fig. 3 **(b, c)**), the CEs and life time of the Cu foil are even lower. The CP-NCNTs always presents the best performances compared to both CP and Cu foil, in which it can be stable for over 130 cycles (CE > 96.7%) and 300 cycles (CE > 98.6%) under the conditions of 1 mA cm^{-2}/3 mAh cm^{-2} and 3 mA cm^{-2}/1 mAh cm^{-2}, respectively. Additionally, when the current density and capacity increase to 3 mA cm^{-2} and 3 mAh cm^{-2}, the CP-NCNTs can deliver an enhanced performance of over 150 cycles while the Cu foil and CP are unstable after only 20 cycles and 100 cycles, respectively (as shown in Fig. 3 **(d)**).

The performance of the Li foil with and without CP-NCNTs interlayers as an anode for LMBs was further investigated in a full cell using C/$LiFePO_4$ as the cathode. The loading of C/$LiFePO_4$ is ~ 10 mg cm^{-2} corresponding to an areal capacity of ~1.7 mAh cm^{-2}. Fig. 3 **(e)** presents the cycling performances of full cells using bare Li foil, Li-CP and Li-CP-NCNTs-3 as the anode at a rate of 1 C (~ 1.7 mA cm^{-2}). In the batteries using bare Li foil, the specific capacity drops to 40 mAh g^{-1} after 150 cycles due to the poor cyclability of the planar Li foil. With one layer of CP as interlayer, the specific capacity keeps around 100 mAh g^{-1} after 150 cycles, indicating the obvious improvement of CP interlayer. However, the cycling stability is still decreasing after 200 cycles with only one layer of CP due to the high loading and areal capacity of LFP. Promisingly, with the CP-NCNTs interlayer, the full cell can maintain a stable capacity of 130 mAh g^{-1} over 150 cycles. The cycling stability and capacity retention demonstrates that the bi-functional CP-NCNTs interlayer can effectively improve the electro-

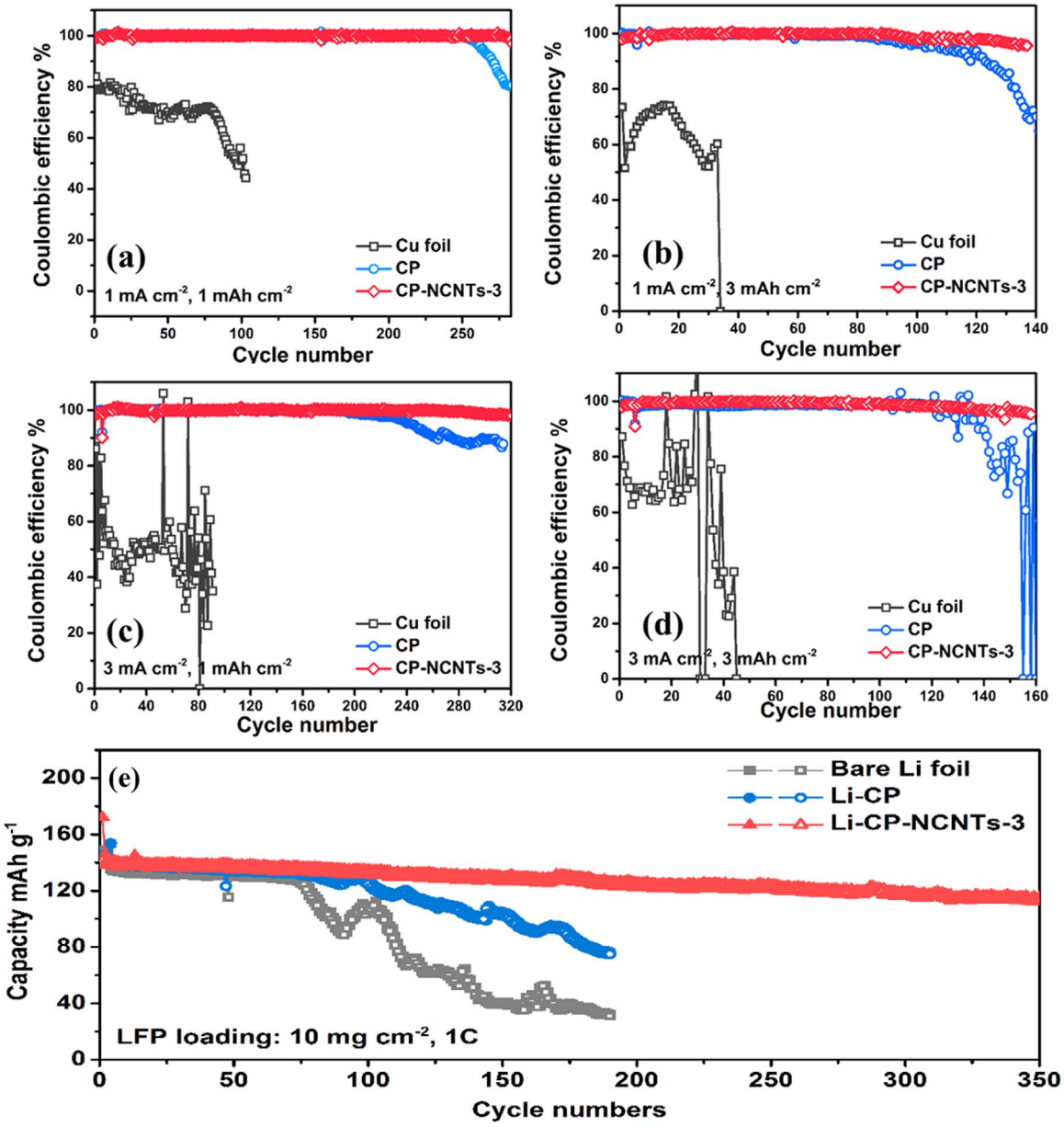

Fig. 3. CE of Li deposition on Cu foil, CP and CP-NCNTs-3 under different cycling conditions: (a) 1 mA cm^{-2} with a capacity of 1 mAh cm^{-2}; (b) 1 mA cm^{-2} with a capacity of 3 mAh cm^{-2}; (c) 3 mA cm^{-2} with a capacity of 1 mAh cm^{-2}; (d) 3 mA cm^{-2} with a capacity of 3 mAh cm^{-2}. (e) Cycling performance of full cells (C/$LiFePO_4$ as cathode) using Li foil, Li-CP and Li-CP-NCNTs as anode at 1 C.

chemical performances compared to the pristine Li foil anode in a full cell format.

To understand the effects of the CP-NCNTs interlayer on the process of Li plating/stripping, the morphologies of deposited Li in different parts of Li-CP-NCNTs composite electrodes are characterized by SEM. It has been widely reported and also observed in our previous works that the serious Li dendrite growth happens on the surface of Li foil due to the inhomogeneous nucleation and growth [36]. At the same time, dead Li layers are formed on the Li surface causing the volume change and large resistance. Fig. S7 shows the SEM images of the CP-NCNTs-3 surface and Li foil surface in the Li-NCNTs-3 composite electrode at different stages of cycling. Different from the large pit formations on the bare Li foil in the first stripping process, it can be obviously seen that the pitting process is avoided (Fig. S7 **(b)**). Furthermore, no mossy and dendritic Li growth on the CP-NCNTs-3 interlayer can be seen (Fig. S7 **(a)**). In addition, during the first plating process, both the surfaces of CP-NCNTs and Li foil are seen to be relatively smooth without any dendritic and mossy Li growth (Fig. S7 **(c, d)**). After 10 cycles of repeated plating/stripping, the surface of CP-NCNTs is uniformly covered with deposited Li and the surface of Li is still very smooth, avoiding Li dendrite growth. The dendrite-free Li deposition is attributed to the uniform local current distributions and homogeneous nucleation and growth of Li caused by the CP-NCNTs interlayers. In addition, the cross-section view SEM images of the CP-NCNTs-3 and Li foil in Li-CP-NCNTs composites are shown in Figs. S8–10. From the cross-section images, it can be observed that the thicknesses of Li foil and CP-NCNTs undergo almost no change in the different cycling stages, such as first stripping **(**Fig. S8**)**, first plating **(**Fig. S9**)** and after 10 cycles of plating/stripping **(**Fig. S10**)**. Moreover, the top-view and cross-section view SEM images of both Li foil and CP-NCNTs-3 in the Li-CP-NCNTs-3 composite electrode after 100 cycles under the current density of 5 mA cm^{-2} and 10 mA cm^{-2} are presented in Fig. S12 and Fig. S13, respectively. From the top-view SEM images in Fig. S12 and Fig. S13, it can be observed that there is no Li dendrite growth on the surface of both Li foil and CP-NCNTs-3 under the high current density up to 10 mA cm^{-2} after 100 cycles. Meanwhile, the

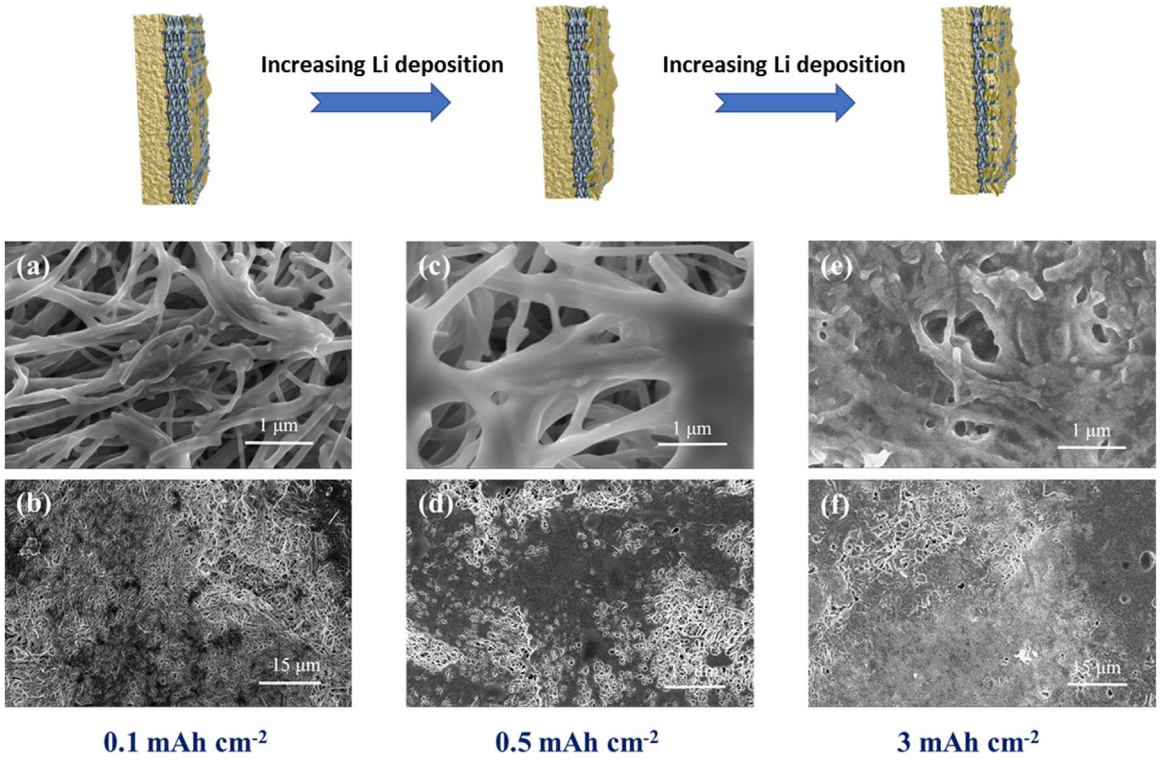

Fig. 4. SEM images of the top surface of CP-NCNTs interlayer after 10 cycles of plating/stripping with different capacities of 0.1 mAh cm^{-2} (a, b), 0.5 mAh cm^{-2} (c, d) and 3 mAh cm^{-2} (e, f).

thickness of CP-NCNTs-3 interlayer remains approximately ~ 450 μm, indicating the minimize volume change of the electrode after 100 cycles. Thus, with the designed interlayer of CP-NCNTs, the bi-functional properties of the dendrite-free Li deposition and minimum volume change has been realized during electrochemical plating/stripping.

To further understanding the Li deposition process, the morphologies of CP-NCNTs interlayers with different Li capacities are also investigated in Fig. 4 and Fig. S11. Fig. 4 **(a, b)** displays the SEM images of CP-NCNTs interlayers after 10 cycles of plating/stripping with a capacity of 0.1 mAh cm^{-2}. It can be seen that the NCNTs are still visible and Li is deposited around the surface of the NCNTs. With a deposition capacity of 0.5 mAh cm^{-2}, the Li is deposited along and between the spaces of the NCNTs (Fig. 4 **(c, d)**). Subsequently, the bulk Li almost encompasses the entire surface of NCNTs in the CP-NCNTs without any Li dendrite formation, as shown in Fig. 4 **(e, f)**. From the cross section view SEM images (Fig. S11), it also can be observed that the volume change of Li is limited in the CP-NCNTs interlayer even with a large capacity of 5 mAh cm^{-2}. Meanwhile, with the large Li deposition amount during cycling, the thicknesses of Li in CP-NCNTs interlayers increase, as shown in Fig. S11. Furthermore, with the CP-NCNTs interlayer on the Li foil, the mossy and dendritic Li deposition can be effectively reduced to achieve a dendrite-free structure. Moreover, the volume change of Li during plating/stripping is confined to the void space of 3D CP-NCNTs. Lastly, the Li is nucleated on the surface of NCNTs and further deposited along the NCNTs and the spaces between them, leading to a reduction in local current and homogeneous Li^+ flux distributions.

3. Conclusion

In conclusion, we extend the “interlayer” concept to the application of Li metal anodes and rationally design a bi-functional interlayer using carbon paper as a base material. The vertical NCNTs are grown on the carbon fibres of CP to obtain a 3D interlayer structure for Li metal. Herein, we firstly demonstrated the relationships between surface area and electrochemical performances for the 3D structure by controlling the growth time of NCNTs during the SPCVD process. Impressively, the Li-CP-NCNTs composite electrode can deliver stable cycling performances for over 600 h (~ 900 cycles) and 250 h (~ 750 cycles) at the high current densities of 5 mA cm^{-2} and 10 mA cm^{-2}, which is two times higher than that of the CP interlayers. Meanwhile, with a high capacity of 3 mAh cm^{-2}, the Li metal electrode with CP-NCNTs interlayer delivers the long life time of over 350 h at a current density of 3 mA cm^{-2}. The morphologies of both Li foil and CP-NCNTs interlayers indicate that the Li dendrite-free deposition and minimum volume change structure can be obtained with the “bi-functional” interlayers. We believe that these new findings could open a new window for the fabrication of safe, long life time, dendrite-free and minimum volume change Li metal anodes.

Acknowledgements

This research was supported by the Natural Science and Engineering Research Council of Canada (NSERC), the Canada Research Chair Program (CRC), the Canada Foundation for Innovation (CFI), and the University of Western Ontario (UWO).

Appendix A. Supplementary material

Supplementary data associated with this article can be found in the online version at doi:10.1016/j.ensm.2018.07.015.

References

[1] A. Zhamu, G. Chen, C. Liu, D. Neff, Q. Fang, Z. Yu, W. Xiong, Y. Wang, X. Wang, B.Z. Jang, Energy Environ. Sci. 5 (2012) 5701–5707.
[2] J.T. Vaughey, G. Liu, J.-G. Zhang, MRS Bull. 39 (2014) 429–435.
[3] W. Xu, J. Wang, F. Ding, X. Chen, E. Nasybulin, Y. Zhang, J.-G. Zhang, Energy Environ. Sci. 7 (2014) 513–537.
[4] Z. Tu, P. Nath, Y. Lu, M.D. Tikekar, L.A. Archer, Acc. Chem. Res. 48 (2015) 2947–2956.

[5] X.B. Cheng, R. Zhang, C.Z. Zhao, F. Wei, J.G. Zhang, Q. Zhang, Adv. Sci. 3 (2016) 1500213.
[6] K. Zhang, G.-H. Lee, M. Park, W. Li, Y.-M. Kang, Adv. Energy Mater. 6 (2016) 1600811.
[7] J. Lang, L. Qi, Y. Luo, H. Wu, Energy Storage Mater. 7 (2017) 115–129.
[8] C. Yang, K. Fu, Y. Zhang, E. Hitz, L. Hu, Adv. Mater. 29 (2017) 1701169.
[9] X.B. Cheng, R. Zhang, C.Z. Zhao, Q. Zhang, Chem. Rev. 15 (2017) 10403–10473.
[10] Y. Guo, H. Li, T. Zhai, Adv. Mater. 29 (2017) 1700007.
[11] D. Wang, W. Zhang, W. Zheng, X. Cui, T. Rojo, Q. Zhang, Adv. Sci. 4 (2017) 1600168.
[12] S. Xin, Y. You, S. Wang, H.-C. Gao, Y.-X. Yin, Y.-G. Guo, ACS Energy Lett. 2 (2017) 1385–1394.
[13] K.N. Wood, M. Noked, N.P. Dasgupta, ACS Energy Lett. 2 (2017) 664–672.
[14] D. Lin, Y. Liu, Y. Cui, Nat. Nanotechnol. 12 (2017) 194–206.
[15] R. Zhang, N.W. Li, X.B. Cheng, Y.X. Yin, Q. Zhang, Y.G. Guo, Adv. Sci. 4 (2017) 1600445.
[16] H. Yang, C. Guo, A. Naveed, J. Lei, J. Yang, Y. Nuli, J. Wang, Energy Storage Mater. 14 (2018) 199–221.
[17] N.W. Li, Y.X. Yin, C.P. Yang, Y.G. Guo, Adv. Mater. 28 (2016) 1853–1858.
[18] E. Kazyak, K.N. Wood, N.P. Dasgupta, Chem. Mater. 27 (2015) 6457–6462.
[19] A.C. Kozen, C.F. Lin, A.J. Pearse, M.A. Schroeder, X. Han, L. Hu, S.B. Lee, G.W. Rubloff, M. Noked, ACS Nano 9 (2015) 5884–5892.
[20] Y. Zhao, L.V. Goncharova, Q. Sun, X. Li, A. Lushington, B. Wang, R. Li, F. Dai, M. Cai, X. Sun, Small Methods 2 (2018) 1700417.
[21] Q. Pang, X. Liang, A. Shyamsunder, L.F. Nazar, Joule 1 (2017) 871–886.
[22] X. Liang, Q. Pang, I.R. Kochetkov, M.S. Sempere, H. Huang, X. Sun, L.F. Nazar, Nat. Energy 6 (2017) 17119.
[23] Y. Zhao, L.V. Goncharova, A. Lushington, Q. Sun, H. Yadegari, B. Wang, W. Xiao, R. Li, X. Sun, Adv. Mater. 29 (2017) 1606663.
[24] Y. Zhao, L.V. Goncharova, Q. Zhang, P. Kaghazchi, Q. Sun, A. Lushington, B. Wang, R. Li, X. Sun, Nano Lett. 17 (2017) 5653–5659.
[25] D. Lin, Y. Liu, Z. Liang, H.W. Lee, J. Sun, H. Wang, K. Yan, J. Xie, Y. Cui, Nat. Nanotechnol. 11 (2016) 626–632.
[26] W. Liu, D. Lin, A. Pei, Y. Cui, J. Am. Chem. Soc. 138 (2016) 15443–15450.
[27] Y. Liu, D. Lin, Z. Liang, J. Zhao, K. Yan, Y. Cui, Nat. Commun. 7 (2016) 10992.
[28] R. Zhang, X.B. Cheng, C.Z. Zhao, H.J. Peng, J.L. Shi, J.Q. Huang, J. Wang, F. Wei, Q. Zhang, Adv. Mater. 28 (2016) 2155–2162.
[29] W. Deng, X. Zhou, Q. Fang, Z. Liu, Adv. Energy Mater. 8 (2018) 1703152.
[30] L. Fan, H.L. Zhuang, W. Zhang, Y. Fu, Z. Liao, Y. Lu, Adv. Energy Mater. 15 (2018) 1703360.
[31] Y. Zhang, W. Luo, C. Wang, Y. Li, C. Chen, J. Song, J. Dai, E.M. Hitz, S. Xu, C. Yang, Y. Wang, L. Hu, PNAS 114 (2017) 3584.
[32] H. Ye, S. Xin, Y.X. Yin, J.Y. Li, Y.G. Guo, L.J. Wan, J. Am. Chem. Soc. 139 (2017) 5916–5922.
[33] Z. Lu, Z. Zhang, X. Chen, Q. Chen, F. Ren, M. Wang, S. Wu, Z. Peng, D. Wang, J. Ye, Energy Storage Mater. 11 (2018) 47–56.
[34] Q. Song, H. Yan, K. Liu, K. Xie, W. Li, W. Gai, G. Chen, H. Li, C. Shen, Q. Fu, S. Zhang, L. Zhang, B. Wei, Adv. Energy Mater. (2018) 1800564. http://dx.doi.org/10.1002/aenm.201800564.
[35] R. Zhang, X. Chen, X. Shen, X.-Q. Zhang, X.-R. Chen, X.-B. Cheng, C. Yan, C.-Z. Zhao, Q. Zhang, Joule 2 (2018) 764–777.
[36] Y. Zhao, Q. Sun, X. Li, C. Wang, Y. Sun, K.R. Adair, R. Li, X. Sun, Nano Energy 43 (2018) 368–375.
[37] Y.S. Su, A. Manthiram, Nat. Commun. 3 (2012) 1166.
[38] Z. Wang, X. Wang, W. Sun, K. Sun, Electrochim. Acta 252 (2017) 127–137.
[39] J. Bobnar, M. Lozinsek, G. Kapun, C. Njel, R. Dedryvere, B. Genorio, R. Dominko, Sci. Rep. 8 (2018) 5819.
[40] H. Yadegari, M.N. Banis, B. Xiao, Q. Sun, X. Li, A. Lushington, B. Wang, R. Li, T.-K. Sham, X. Cui, X. Sun, Chem. Mater. 27 (2015) 3040–3047.